

## Formation and in vitro induction ability of apatite nanobelt coating on silicon

WU Zhen-jun(吴振军)<sup>1</sup>, YUAN Jian-min(袁剑民)<sup>2</sup>, LI Wen-sheng(李文生)<sup>1</sup>,  
REN Yan-qun(任艳群)<sup>1</sup>, CHEN Zong-zhang(陈宗璋)<sup>1</sup>

1. College of Chemistry and Chemical Engineering, Hunan University, Changsha 410082, China;
2. College of Materials Science and Engineering, Hunan University, Changsha 410082, China

Received 29 September 2009; accepted 20 April 2010

**Abstract:** Apatite coating with nanobelt structure was fabricated on single crystal silicon by a two-step method of electrodeposition at 1.0–2.0 mA/cm<sup>2</sup> with DC power and vapor-thermal treatment (VTT) at 150–180 °C for 6 h over alkali medium. Scanning electron microscopy (SEM), X-ray diffractometry (XRD), and electron diffraction spectrometry (EDS) were employed to investigate the compositions and morphologies of specimens before or after vapor-thermal treatment. The results demonstrate that nanobelt crystals of coating, 0.5–2 μm in width, 100 nm in thickness, and 6–10 μm in length, are Ca-deficient apatite (CDA) with a mole ratio of Ca to P approximately of 1.60, which shows similarity of the nanobelt coating to inorganic phase in composition and to collagen in dimension appearing in human hard tissue. Induced nucleation and growth of bone-like apatite were observed on the nanobelt after soaking in a simulated body fluid (SBF) for 6 h and for 3 d, respectively, identifying that nanobelt has good ability for induction of bone-like apatite in SBF.

**Key words:** apatite; nanobelt; electrodeposition; vapor-thermal treatment; silicon

### 1 Introduction

As the main inorganic component of human bone and tooth, apatite (especially hydroxyl-apatite, HA) has served as the most important bio-medical material due to its excellent biocompatibility[1–5]. Nano- and micro-metric apatites cover many fields including hard tissue implants, wearable biocoating, controllable drug-release carrier, water and air purificant and so on. Also, HA coating has attracted much interest for biodevices based on silicon technologies, such as biochips, biosensors, and micro-electro-mechanical systems (BIOMEMS) applied to medical diagnosis and treatments since biocompatible HA can facilitate their in vivo fixation and protect them from the erosion caused by body fluid[6–8].

So far, synthetic apatite shows various morphologies such as nano-rods, nano-strings, nano-plates, and nano-spheres. And now, it is highly interesting that biomimic apatite can be synthesized holding composition close to natural bone apatite and morphology matching with collagen, respectively[9–13]. Since 1991, electrocrystallization (electrodeposition) has

been developed to fabricate biocompatible coatings on bio-medical metals by carrying out cathodic-electrolysis using a mode of constant current or constant potential in electrolyte containing calcium and phosphorus salts[14]. Generally, plate-like CaHPO<sub>4</sub>·2H<sub>2</sub>O (DCPD) micro-crystals form at high potential or current density in electrolyte of calcium and phosphorus salts with high concentrations[15]. However, DCPD has poor chemical stabilization and biocompatibility because it is highly soluble in body fluid, so a transformation of DCPD to biocompatible TCP or HA is necessary by subsequent calcination, hot-alkali immersing, or hydrothermal treatment[16–20]. And simultaneously, micro plates are converted into nanorods or nanostrings. It is also reported that pure nano-HA can be fabricated on bio-medical metals by a hybrid method of electrodeposition and hydrothermal treatment at high temperature and pressure in an autoclave, and improved adhesion strength between coating and substrate is obtained in case that ultra-fine TiO<sub>2</sub> powder is co-deposited with HA[21]. In addition, direct formation of flower-like and inter-connecting porous nanometric HA biocoating is realized at 85–100 °C and pH of 5–7 in electrolyte with very low concentration[22].

In this work, apatite coating with nanobelt structure is successfully fabricated on single crystal silicon by a two-step method including electrodeposition in electrolyte dissolved with millimole calcium and phosphorus salts and vapor-thermal treatment (here called vapor-thermal treatment, VTT) over alkali medium in an autoclave. Morphologies and compositions of nanobelt apatite coating were characterized by scanning electron microscopy (SEM), X-ray diffractometry (XRD), and electron diffraction spectrometry (EDS). In vitro induction of bone-like apatite on as-obtained nanobelt apatite coating was tested for soaking specimens in a simulated body fluid (SBF).

## 2 Experimental

### 2.1 Fabrication and SBF-soaking of specimens

The procedure for fabricating specimens included electrodeposition, vapor-thermal treatment and drying. All chemicals used are of analytical grade.

#### 1) Electrodeposition

The electrolyte for electrodeposition was an aqueous solution containing  $7.5 \times 10^{-3}$  mol/L  $\text{Ca}(\text{NO}_3)_2$  and  $3.8 \times 10^{-3}$  mol/L  $\text{NaH}_2\text{PO}_4$ . Its pH value was adjusted to 5.1 by 0.1 mol/L NaOH solution. Electrodeposition was performed at constant current densities ranging from 1.0 to 2.0 mA/cm<sup>2</sup> and 50 °C for 30 min with mild magnetic stirring. The cathode (working electrode) was silicon (111) and the anode (counter electrode) was a graphite rod. The electrodeposition DC power was a electrophoresis apparatus (DYY-6B, Beijing).

#### 2) Vapor-thermal treatment and drying

After electrodeposition, specimens were rinsed by deionized water and then subjected to hot vapor over a 5% NaOH solution vertically at 150–180 °C for 6 h in an autoclave. VTT specimens were rinsed by deionized water again and dried at 100 °C for 3 h.

All obtained specimens were finally soaked in a simulated body fluid for different time to investigate their in vitro inductive ability of bone-like apatite. Compositions and preparation of SBF were seen in Refs.[23–24].

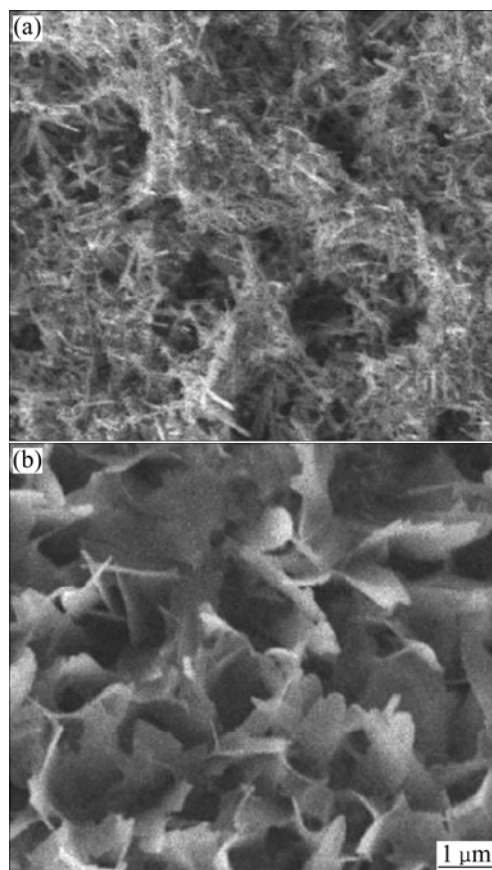
### 2.2 Characterization and analysis

The morphologies of specimens were characterized by field-emission scanning electron microscopy (FESEM, JEOL/JSM-6700, Japan) at an acceleration voltage of 5 kV. X-ray diffractometry (XRD, Siemens D5000, Germany) was conducted to analyze phases of the obtained coatings on silicon using  $\text{Cu K}_\alpha$  radiation at a voltage of 35 kV with a current of 30 mA and a scanning rate of 0.02 (°)/s. The elements and their mole fractions of the pre- and post-soaking specimens in SBF were

determined by electron diffraction spectrometry (EDS, OXFORD INCA, British) attached to SEM.

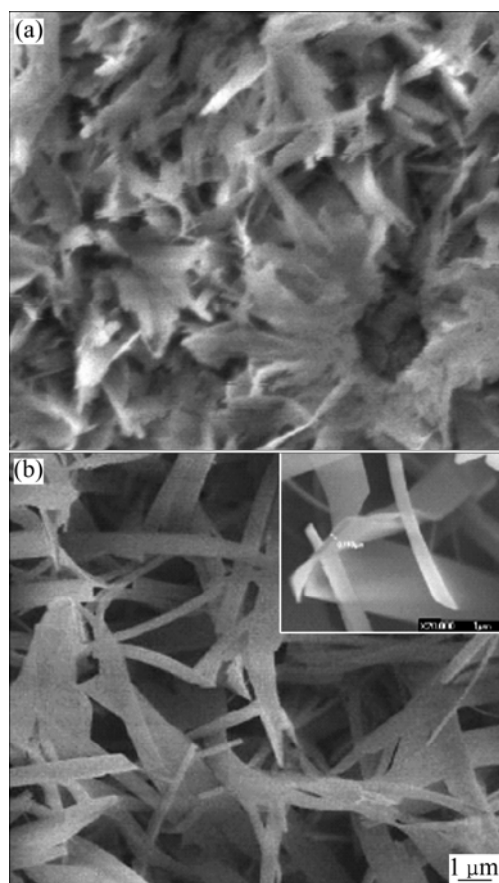
## 3 Results and discussion

Fig.1 shows the morphologies of electrodeposits on silicon formed at different current densities. The 1.0 mA/cm<sup>2</sup> deposited coating on silicon consists of rods and pieces as shown in Fig.1(a). Herein the rods are 1–3 μm in length and 20–50 nm in diameter and the pieces are 0.8–1.5 μm in length and 200 nm in thickness. During cathode electrodeposition at low current density in very diluted electrolyte, *c*-axis of calcium phosphates such as DCPD and Ca-deficient apatite is the favorable growth direction, which results in needle-like electrodeposits [21–22]. While subjected to high current densities and high electrolyte concentrations, both of *c*-axis and *b*-axis become the preferential directions of oriented growth of electrodeposits, especially plate-like electrodeposits can form with growth along *a*-axis when both of current density and electrolyte concentration are high enough [12]. In the present work, it is shown in Fig.1(b) that, after electrodeposition at 2.0 mA/cm<sup>2</sup> in diluted electrolyte, the coating is mostly composed by interconnecting lamellar-like crystals with thickness of 50 nm and width of 2 μm except for a few of nanostrings.



**Fig.1** Morphologies of electrodeposits on silicon formed at 1.0 mA/cm<sup>2</sup> (a) and 2.0 mA/cm<sup>2</sup> (b)

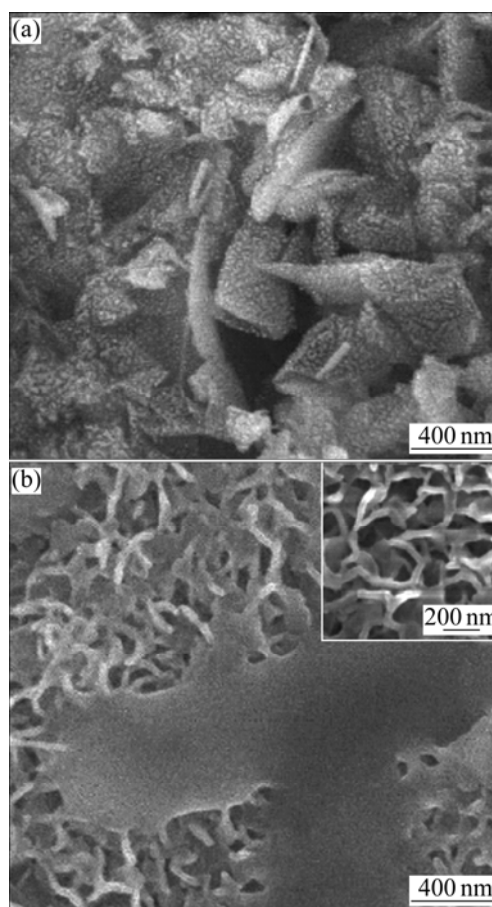
Fig.2 shows the morphologies of the coating electrodeposited at  $1.0 \text{ mA/cm}^2$  after being subjected to hot vapor over alkali medium at  $150 \text{ }^\circ\text{C}$  and  $180 \text{ }^\circ\text{C}$  for 6 h in an autoclave. It can be seen from Fig.2(a) that rods and pieces become cingulum-like structure with  $150 \text{ }^\circ\text{C}$  vapor-thermal treatment, and from Fig.2(b) nanobelts can be obviously observed on silicon after treatment at  $180 \text{ }^\circ\text{C}$ . These nanobelts are inter-textured and possess width of  $0.5\text{--}2 \text{ }\mu\text{m}$  and length of  $6\text{--}10 \text{ }\mu\text{m}$ , and their thickness is approximately  $100 \text{ nm}$  according to the inset in Fig.2(b). Compared with micrometric block DCPD and nanometric needle-like HA deposited from electrolytes with high concentration and low concentration, respectively, the nanobelt crystals presented in this work are closer to collagen in hard tissues in dimension[1, 25], and it is also expected that naturally textured nanobelt crystals can match with hard tissue in mechanical performances.



**Fig.2** Morphologies of vapor-thermally treated electrodeposits at  $1.0 \text{ mA/cm}^2$  on silicon at  $150 \text{ }^\circ\text{C}$  (a) and  $180 \text{ }^\circ\text{C}$  (b)

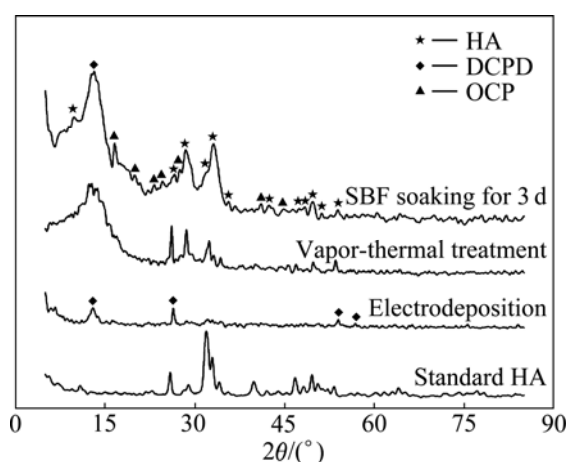
Fig.3 shows the morphologies of the specimens electrodeposited at  $1.0 \text{ mA/cm}^2$  and vapor-thermally treated at  $180 \text{ }^\circ\text{C}$ , after soaking in SBF for 6 h and 72 h (3 d). With a duration of 6 h in SBF, nanospheres,  $10\text{--}20 \text{ nm}$  in diameter, have almost covered the surface of nanobelts, as shown in Fig.3(a). These nanospheres seem

to be nuclei of apatite derived from the enrichment and mineralization of calcium and phosphorus in SBF. After soaking for 3 d, irregular porous ball-like structure with diameter of  $1\text{--}2 \text{ }\mu\text{m}$  has fully coated the specimen, as seen from Fig.3(b). And a magnified image, the inset in Fig.3(b), demonstrates that these irregular balls form by  $20 \text{ nm}$  strings, which are linked to network and similar to that of bone apatite. The nanobelt crystals on silicon show good inductive ability in SBF according to the quick nucleation and growth of bone-like apatite observed from Fig.3.



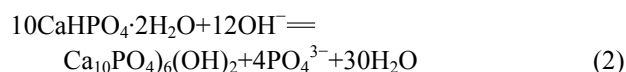
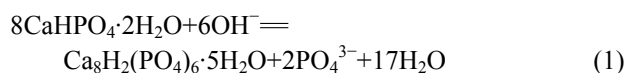
**Fig.3** Morphologies of SBF-soaking specimens for 6 h (a) and 3 d (b) (Specimens formed by electrodeposition at  $1.0 \text{ mA/cm}^2$  and subsequent vapor-thermal treatment at  $180 \text{ }^\circ\text{C}$ )

Fig.4 and Fig.5 show the XRD and EDS results of the specimens electrodeposited at  $1.0 \text{ mA/cm}^2$  and vapor-thermally treated at  $180 \text{ }^\circ\text{C}$ , after soaking in SBF for 3 d, respectively. It is found that DCPD is formed after electrodeposition on the basis of diffraction peaks at  $13.8^\circ$ ,  $26.4^\circ$ ,  $53.5^\circ$ , and  $57.4^\circ$  in Fig.4, especially the diffraction peak at  $26.4^\circ$  is a typical peak corresponding to DCPD as described by Refs.[14, 17]. In addition, weak diffraction peaks between  $30.5^\circ$  and  $33.5^\circ$  are also observed from Fig.4, suggesting that apatite is contained in electrodeposits, and widened diffraction peaks may be due to low crystallinity of coating or nano-structure as



**Fig.4** XRD spectra of standard HA and specimens after electrodeposition at  $1.0 \text{ mA/cm}^2$ , vapor-thermal treatment at  $180^\circ\text{C}$ , and SBF soaking for 3 d, respectively

shown in Fig.1(a). After vapor-thermal treatment, obvious and intensified diffraction peaks of apatite at  $30.8^\circ$ ,  $32.3^\circ$ ,  $33.1^\circ$  can be seen from Fig.4, which identifies that nanobelt coating in Fig.2(b) is composed of apatite and the crystallinity of coating is improved. It is suggested that octacalcium phosphate ( $\text{Ca}_8\text{H}_2(\text{PO}_4)_6 \cdot 5\text{H}_2\text{O}$ , OCP) formed according to some weak diffraction peaks ranging from  $15^\circ$  to  $28^\circ$  given by the XRD spectrum of the specimen obtained after VTT. In alkaline vapor medium, DCPD may react with  $\text{OH}^-$  and  $\text{H}_2\text{O}$  and then form OCP and HA as



Obviously, Eq.(1) and Eq.(2) are rivals in consumption of  $\text{OH}^-$ . However, HA, the product of Eq.(2), is more thermodynamically stable than OCP produced by Eq.(1)[4]. Furthermore, HA crystals contained in the electrodeposits can serve as the seeds for HA nucleation and growth from Eq.(2). The formation of lengthwise HA nanobelts may be contributed by the simultaneous growth of crystals along  $c$ -axis and  $b$ -axis, especially the  $c$ -axis is the most preferential growth direction.

According to the spectra in Fig.4, the SBF-soaking inductive layer on nanobelt coating has widened diffraction peaks of apatite compared with those of standard HA, which may be caused by the low crystallinity and nanophase of newly formed layer, but it is further confirmed that the obtained nanobelt apatite coating on silicon has excellent inductive ability for the formation of bone-like apatite in vitro. In Fig.4, OCP diffraction peaks can also be observed after SBF soaking

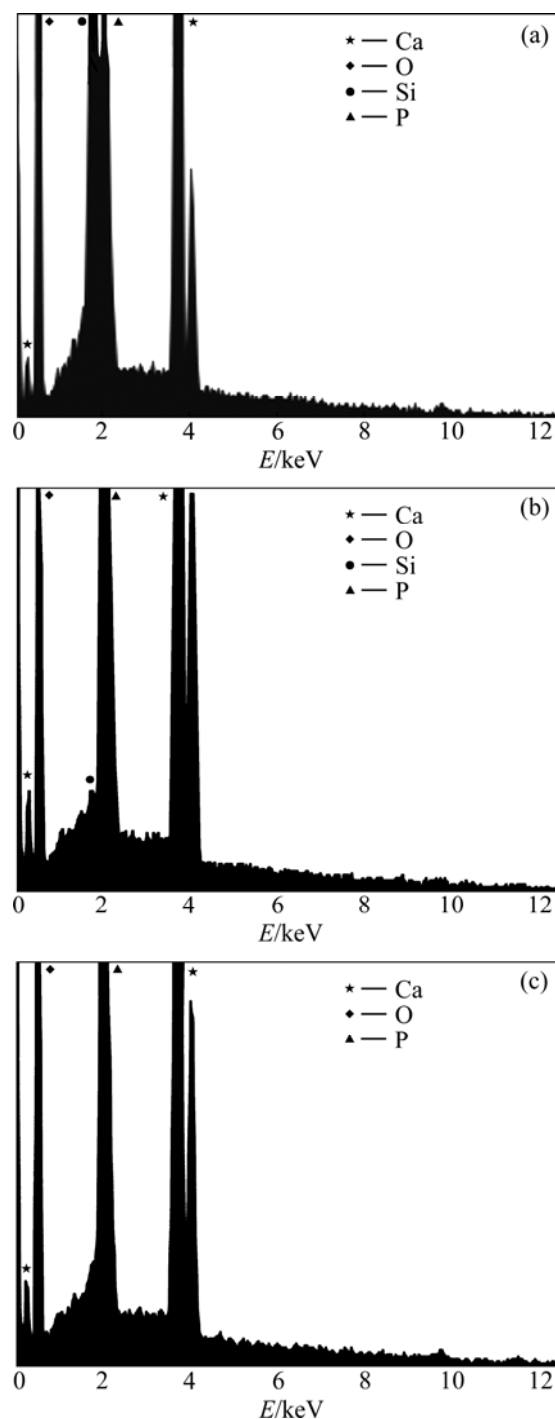


**Fig.5** EDS results of specimens after electrodeposition at  $1.0 \text{ mA/cm}^2$  (a), vapor-thermal treatment at  $180^\circ\text{C}$  (b), and SBF soaking for 3 d (c), respectively

for 3 d. IJIMA et al[26–27] elucidated that lamellar OCP forms at the initial inductive stage and subsequently acts as a template for the nucleation and growth of bone-like apatite.

Fig.5(a) shows a mole ratio of Ca to P of 1.19 of electrodeposits, which is lower than 1.67, the stoichiometric mole ratio of Ca to P in hydroxyl-apatite. This should be due to DCPD, holding a mole ratio of Ca to P of 1, and apatite coexisting in electrodeposits.

Ca-deficient apatite (CDA) with a mole ratio of Ca to P of 1.60 forms from electrodeposits after vapor-thermal treatment. And 3 d SBF soaking resultant precipitates are also CDA with a mole ratio of Ca to P of 1.62 derived from the higher mole ratios of Ca to P of OCP and HA and are similar to inorganic phase in human hard tissue [3–4, 6–9].

## 4 Conclusions

1) The direct preparation of nanobelt apatite coating on single crystal silicon is accomplished by combining electrodeposition and subsequent vapor-hydrothermal treatment over diluted alkaline solution. During VTT, HA nanobelts form due to the crystal growth along lengthwise *c*-axis and *b*-axis prior to OCP with lower thermodynamic stability. OCP is the initially formed phase and can serve as a template for the nucleation and growth of HA by soaking VTT-resulted HA nanobelt coating in SBF.

2) As-obtained VTT coating is composed of Ca-deficient apatite (CDA) crystals with a mole ratio of Ca to P of approximately 1.60 and irregular texture-like nanobelt structure. It is expected that this nanobelt intertexture can find its application in developing new type of biomimic composites with bio-organic matter such as collagen fibers based on their similarity in dimension.

## References

- [1] YAO Kang-de, YIN Yu-ji. Biomaterials for tissue engineering [M]. Beijing: Chemical Industry Press, 2003: 1–18. (in Chinese)
- [2] KIM H. Bioactive ceramics: Challenges and perspectives [J]. J Ceram Soc Jpn, 2001, 109(4): 49–57.
- [3] GU Y, KHOR K, CHEANG A. Activity of plasma sprayed yttria stabilized zirconia reinforced hydroxyapatite/Ti6Al4V composite coatings in simulated body fluid [J]. Biomaterials, 2004, 25(6): 3177–3185.
- [4] HENCH L. Bioceramics: From concept to clinic [J]. J Am Ceram Soc, 1991, 74(6): 1487–1510.
- [5] BEN N, MILEV A, VAGO R. Morphology of sol-gel derived nano-coated coralline hydroxyapatite [J]. Biomaterials, 2004, 25(8): 4971–4975.
- [6] LIU X, FU R, POON R, CHEN P, CHU P, DING C. Biomimetic growth of apatite on hydrogen-implanted silicon [J]. Biomaterials, 2004, 25(25): 5575–5581.
- [7] CHEN S, ZHU Z, ZHU J, ZHANG J, SHI Y, YU K, WANG W, WANG X, FENG X, LUO L, SHAO L. Hydroxyapatite coating on porous silicon substrate obtained by precipitation process [J]. App Surf Sci, 2004, 230(1/2/3/4): 418–424.
- [8] CHUNG R, HSIEH M, PANDA R, CHIN T. Hydroxyapatite layers deposited from aqueous solutions on hydrophilic silicon substrate [J]. Surf Coat Technol, 2003, 165(2): 194–200.
- [9] LIN X, LI X, FAN H, WEN X, LU J, ZHANG X. In situ synthesis of bone-like apatite/collagen nano-composite at low temperature [J]. Materials Letters, 2004, 58(6): 3569–3572.
- [10] LANDI E, CELOTTI G, LOGROSCINO G, TAMPIERI A. Carbonated hydroxyapatite as bone substitute [J]. J Euro Ceram Soc, 2003, 23(10): 2931–2937.
- [11] SHIRTLIFF V J, HENCH L L. Bioactive materials for tissue engineering, regeneration and repair [J]. J Mater Sci, 2003, 38(3): 4697–4707.
- [12] BURG K J, PORTER S, KELLAM J F. Biomaterial developments for bone tissue engineering [J]. Biomaterials, 2000, 21(3): 2347–2359.
- [13] MEDTECH Insight. Orthopaedic biomaterials market review [EB/OL]. <http://www.azom.com>. [2002-01-10].
- [14] SHIRKHAZADEH M. Bioactive calcium phosphate coatings prepared by electrodeposition [J]. J Mater Sci Lett, 1991, 10(6): 1415–1417.
- [15] SHIRKHAZADEH M. Calcium phosphate coatings prepared by electrocrystallization from aqueous electrolytes [J]. J Mater Sci: Mater in Med, 1995, 6(1): 90–93.
- [16] KUMAR M, DASARATHY H, RILEY C. Electrodeposition of brushite coatings and their transformation to hydroxyapatite in aqueous solutions [J]. J Biomed Mater Res, 1999, 45(4): 302–310.
- [17] HAN Y, FU T, XU K. Characterization and stability of hydroxyapatite coatings prepared by an electrodeposition and alkaline-treatment process [J]. J Biomed Mater Res, 2001, 54(1): 96–101.
- [18] WU Z, HE L, CHEN Z. Fabrication and characterization of hydroxyapatite/Al<sub>2</sub>O<sub>3</sub> composite biocoating on titanium [J]. Transactions of Nonferrous Metals Society of China, 2006, 16(2): 259–266.
- [19] MANSO M, JIMENEZ C, MORANT C, HERRERO P, DUART J. Electrodeposition of hydroxyapatite coatings in basic conditions [J]. Biomaterials, 2000, 21(6): 1755–1761.
- [20] YEN S, LIN C. Cathodic reactions of electrolytic hydroxyapatite coating on pure titanium [J]. Mater Chem and Phy, 2003, 77(1): 70–76.
- [21] HU H, LIN C, HU R, LENG Y. A study on hybrid bioceramic coatings of HA/poly(vinyl acetate) co-deposited electrochemically on Ti-6Al-4V alloy surface [J]. Mater Sci Eng C, 2002, 20(1/2): 209–214.
- [22] XIAO X, LIU R, ZHENG Y. Characterization of hydroxyapatite/titania composite coatings codeposited by a hydrothermal-electrochemical method on titanium [J]. Surf Coat Technol, 2006, 200(14/15): 4406–4413.
- [23] WU Zhen-jun, HE Li-ping, CHEN Zong-zhang. Morphology and indirect inductive ability for calcium phosphate coatings of porous aluminum oxide synthesized in different electrolytes [J]. J Chin Ceram Soc, 2004, 32: 1178–1183. (in Chinese)
- [24] WU Zhen-jun, HE Li-ping, CHEN Zong-zhang. Fabrication and in vitro performance of anodic alumina containing calcium [J]. The Chinese Journal of Nonferrous Metals, 2005, 15(10): 1572–1576. (in Chinese)
- [25] WANG R, CUI F Z, LU H, WEN H, MA C, LI H. Synthesis of nanophase hydroxyapatite/collagen composite [J]. J Mater Sci Lett, 1995, 14(6): 490–492.
- [26] IJIMA M, TOHDA H, MORIWAKI Y. Growth and structure of lamellar mixed crystals of octacalcium phosphate and apatite in a model system of enamel formation [J]. J Crystal Growth, 1992, 116(3/4): 319–326.
- [27] IJIMA M, MORIWAKI Y. Lengthwise and oriented growth of octacalcium phosphate crystal in polyacrylamide gel in a model system of tooth enamel apatite formation [J]. J Crystal Growth, 1998, 194(1): 125–132.

(Edited by LI Xiang-qun)